coalescence and redispersion of dilute aqueous dispersions in toluene in a stirred-tank system. A simple coalescence model has been advanced for purposes of estimating the magnitude of the coalescence frequency. This model assumes a constant drop size in the system, a constant number of drops, and a constant coalescence frequency for a fixed set of experimental conditions. The coalescence frequency is defined as the fraction of all drops coalescing per unit time. The experimental results indicate that the coalescence frequency varies as the 2.4 power of the impeller speed and as the square root of the dispersed-phase volume.

ACKNOWLEDGMENT

Exploratory studies on this problem were carried out at the Laboratorium voor Physische Technologie, Technische Hogeschool, Delft, Holland, under a Guggenheim Fellowship held by A. J. Madden. This assistance is gratefully acknowledged as well as the helpful advice of Professor H. Kramers and his students at Delft. Later work was supported by grant G-12137 from the National Science Foundation.

NOTATION

a = interfacial area per drop, sq. cm.

c = concentration of iodine in toluene at time t, g./cc.

c_o = initial concentration of iodine in toluene, g./cc.

c_s = concentration of hypo in aqueous phase, g. $Na_2S_2O_3 \cdot 5H_2O$/cc.

c_{so} = initial concentration of hypo in aqueous phase, g. $Na_2S_2O_3 \cdot 5H_2O$/cc.

I = ionic strength of dispersed phase

k = mass transfer coefficient, cm./sec.

N = total number of drops of dispersed phase ($= N_s + N_w$)

N_s = number of drops containing hypo at time t

N_{so} = initial number of drops containing hypo

N_w = number of drops containing only inert solute at time t

t = time, sec.

S = impeller speed, rev./min.

V_d = total volume of dispersed phase, cc.

V_t = total volume of toluene (continuous) phase, cc.

X = initial ratio of hypo to inert drops $\left(= \frac{N_{so}}{N - N_{so}} \right)$

θ = coalescence frequency, sec.$^{-1}$

LITERATURE CITED

1. Fujinawa, K., and T. Maruyama, *Chem. Eng. (Japan)*, **21**, 75 (1957).
2. Groothuis, H., and F. J. Zuiderweg, *Chem. Eng. Sci.*, **12**, 288 (1960).
3. Johnson, H. F., and Harding Bliss, *Trans. Am. Inst. Chem. Engrs.*, **42**, 331 (1946).
4. Logsdail, D. H., J. D. Thornton, and H. R. C. Pratt, *Trans. Inst. Chem. Engrs. (London)*, **35**, 301 (1957).
5. Moore, W. J., "Physical Chemistry," 2 ed., p. 457, Prentice-Hall, Englewood Cliffs, New Jersey (1955).
6. Parrett, O. W., *IDO-14486*, Phillips Petroleum Company, Atomic Energy Division, Idaho Falls, Idaho
7. Rietema, K., *Chem. Eng. Sci.*, **8**, 103 (1958).
8. Sachs, J. P., and J. H. Rushton, *Chem. Eng. Progr.*, **50**, 597 (1954).
9. Vermeulen, Theodore, G. M. Williams, and G. F. Langlois, *ibid.*, **51**, 85-F (1955).

Manuscript received December 6, 1960; revision received September 11, 1961; paper accepted September 13, 1961.

Axial Solid Distribution in Gas-Solid Fluidized Beds

LIANG-TSENG FAN, CHAU JEN LEE, and RICHARD C. BAILIE

Kansas State University, Manhattan, Kansas

γ-ray attenuation method was applied to determine the axial fluidizing bulk density profile for an air-solid aggregative fluidized bed. Except for beds fluidized at very high air velocities two distinct density zones were noted. The density of the bed in the lower portion of the column was relatively constant for a particular set of operating conditions and did not vary with bed height. The density in the top portion of the bed fell rapidly with bed height.

The average density of the lower zone was correlated as a function of the operating variables. The density in the top zone was represented by a one-tail normal distribution curve. A somewhat better correlation was obtained by a two-parameter equation at high air velocities. The effects of operational variables, such as air velocity, static bed height, particle size, and particle-size distribution on these correlations were investigated.

Friction-factor correlations based on two different definitions of bed height were also obtained.

The major purpose of the present work was to investigate the axial distribution of the fluidized bulk density in an aggregative fluidized bed by γ-ray technique.

During the past years the characteristics of aggregative fluidized beds were studied by several different experimental methods.

1. High speed photographic studies were made by Matheson et al. (*13*), Furukawa and Omae (*9*), and by Massimilla and Westwater (*12*). They took high-speed photographs of bubbles through transparent walls of fluidized columns for gas-solid systems.

2. Shuster and Kisliak (*18*) studied the uniformity of aggregative fluidized beds by using diaphragm plates to measure pressure gradients.

3. Morse and Ballou (*16*) and Dotson (*7*) examined the uniformity of aggregative fluidization by measuring the variation of the electric capacitance between condenser probes. Later Bakker and Heertjes (*4*) applied a similar technique to measure the point porosity of fluidized beds.

4. Yasui and Johanson (*19*) devised a small light probe to study the frequency, thickness, and the rising speed of bubbles in aggregative fluidized beds.

Table 1. Particle Size of Glass Beads Used

Mesh	Particle range	Average size
40-45 U.S. mesh	0.00138-0.0164 in.	0.0153 in.
80-100 U.S. mesh	0.0049-0.0070 in.	0.00642 in.
60-70 U.S. mesh	0.0083-0.0098 in.	0.00906 in.

Chau Jen Lee is at Oklahoma State University, Stillwater, Oklahoma.

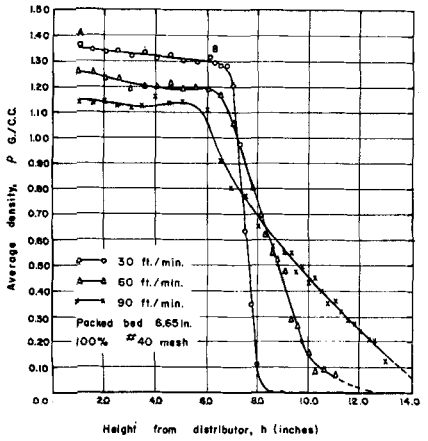

Fig. 1. Effect of air velocity upon the density profiles.

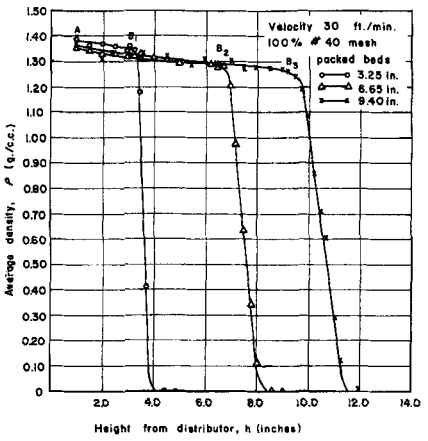

Fig. 2. Effect of static bed height upon density profiles.

5. The X-ray absorption technique made it possible for Grohse (*10*) to measure the over-all density of the aggregative fluidized bed without disturbing the bed. Baumgarten and Pigford (*5*) employed a γ-ray absorption technique in the study of bubble size and bubble frequency in aggregative fluidized beds. Bailie, et al. (*1, 2*) employed the γ-ray technique to measure instability of the aggregative fluidized beds.

Some of these investigators have proposed mathematical or empirical models to fit their experimental data. None of these models has as yet been verified as acceptable and applicable to describe the nonuniform distribution of solid particles in axial direction in aggregative fluidized beds.

The fluidized bed density can be considered to be represented by a lower zone where there is a small change of density and the upper zone where the density falls rapidly with an increase in bed height. These zones are correlated as a function of the operating variables, air velocity, static bed height, particle size, and particle-size distribution. Friction-factor correlations were obtained, based on two different definitions of bed height.

EXPERIMENTAL

Application of γ-ray absorption technique to a fluidized bed is based on the fact that γ radiation from a radioactive source is attenuated by the bed depending upon the local bed density. The attenuation is given by

$$\frac{I}{I_o} = be^{-\mu_m D} \qquad (1)$$

If b is known, the line average density in the fluidized bed can be measured for each axial position by measuring the radiation attenuation and coverting it to density by Equation (1). The buildup factor is a function of several variables and could not be calculated with the desired accuracy. For this reason the buildup factor was determined experimentally against beds of known density. The equipment is described in detail in recent papers by Bailie, et al. (*1, 2*). The same experimental arrangement and equipment was used in this investigation except that a 30-sec. time constant was used for the rate meter.

The particles used in this experiment were glass beads. To minimize error due to size distribution when narrow-cut particles were investigated, the glass beads were reclassified (Table 1).

RESULTS*

General Observations

Typical axial solid distribution profiles of a gas-solid fluidized bed are shown in Figures 1 and 2. Similar profiles were obtained for all experimental runs for different static bed heights and under different air velocities and for mixed particles beds. Two distinct zones can be found in this typical distribution curve: in the range AB of Figure 1 the solid density changes slowly with bed height. After point B the solid density decreases sharply as the distance from the bottom of the bed increases. Each curve was graphically integrated in order to check the accuracy of measurement by means of a material balance.

These typical density profiles show qualitatively the properties of gas-solid fluidized beds under the effect of several operational variables:

Effect of Air Velocity

Figure 1 shows the effect of air velocity upon the fluidized bulk-density profiles. It shows that the density in the lower density zone decreased with increasing air velocity, and the slope of the falling density zone becomes smaller as the air velocity increases. This was expected since more air was passing through the bed at higher air velocity, and therefore the bed was expanded.

Figure 1 also indicates that this two-zone profile becomes less apparent as the air flow rate increases. At flow rate over 90 ft./min. the line-average density falls from the bottom of the bed to the top layer of the fluidizing bed. In other words when the air velocity is low the constant density zone clearly exists, and the bed is closer to the ideally expanded fixed bed (*1*). If the air velocity is high, the air which carries the particles becomes more turbulent and the particles are in more vigorous and randomized movement. Under these conditions of more random motion there is a more gradual and less sharp transition between the density regions.

Effect of Static Bed Height

Figures 3 (a and b) are the typical dimensionless axial density profiles, in which ρ/ρ_{pa} is plotted against h/L_{mf}. These graphs show that the static bed effect on the density profile is relatively small. The dimensionless density profiles for different static bed heights fluidizing at the same air velocity can be approximated by a single curve, especially at low velocity. The deviation from the common dimensionless density profile becomes more significant for the individual profile corresponding to the smallest bed height.

The ratio of the static bed height to the column diameter instead of the static bed height itself is probably the significant variable affecting the bed expansion and the axial particle-distribution profile. This is probably due to the combination of entrance and wall effects. When the bed is shallow and the ratio is small, the air passing through could hardly have time to form well-shaped bubbles before it leaves the fluidizing bed. The two phases of fluidization for the shallow bed are therefore not as pronounced as in the case of deep static bed.

Effect of Particle Size and Bed Composition

The effect of particle size and bed composition were found to have definite effects on the axial particle distribution profiles. These results are consistent with the findings of Dotson (*7*) and Baumgarten and Pigford (*5*).

ANALYSIS OF DATA AND CORRELATIONS

As mentioned in the previous section the axial-density profiles may be divided into a lower-density zone and a falling-density zero. The correlation of the density profile as a function of the operational variables will be obtained for the two zones separately. It may be considered (*3*) that the lower-density zone extends from the bottom of the bed to the position corresponding to the static bed height before fluidization, and the falling-density zone exists above the static bed height.

Bed Density Correlation in the Lower-Density Zone

The density in the lower-density zone is fairly constant. From the qualitative observation made in the previous section the air velocity is the major factor affecting the shape of the

* Tabular material has been deposited as document 7076 with the American Documentation Institute, Photoduplication Service, Library of Congress, Washington 25, D. C., and may be obtained for $5.00 for photoprints or $2.25 for 35-mm. microfilm.

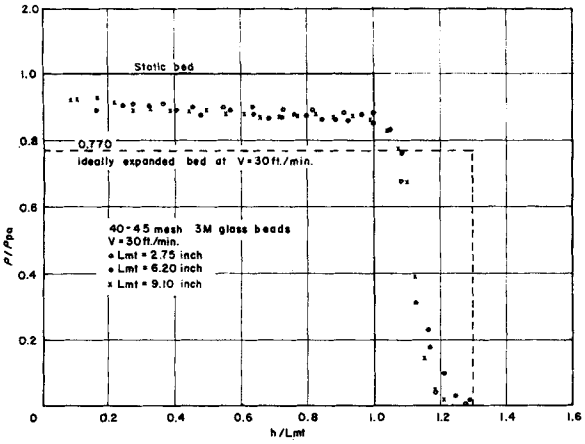

Fig. 3a. Dimensionless density profile at $V = 30$ ft./min. for various static bed heights.

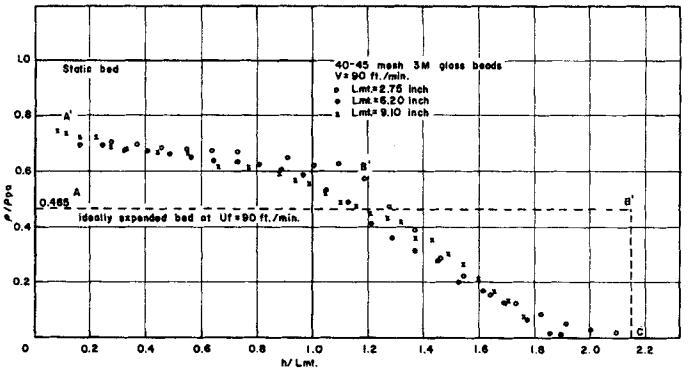

Fig. 3b. Dimensionless density profile at $V = 90$ ft./min. for various static bed heights.

density profile, whereas the static bed height has little effect. Thus the density in the constant-density zone can be correlated as a function of air velocity and particle diameter.

The average density of the lower-density zone (where the zone ranges from the bottom of the column to the position corresponding to the static bed height) can be obtained from

$$\bar{\rho}_d = \frac{M_{s_2}}{SL_{mf}} \tag{2}$$

The mass of the particles in the falling density zone is

$$M_{s_1} = M - M_{s_2} \tag{3}$$

It was indicated by Bakker et al. (3) that the volume of these particles suspended in the space above L_{mf} corresponds to the product of the volume of the gas bubbles appearing below L_{mf} and the particle concentration in the prefluidized state. Thus

$$\text{Vol}_{s_1} = (1 - \epsilon_{mf})\text{Vol}_b \tag{4}$$

If S' is the part of area A which is occupied by the dense-phase emulsion, $(S - S')$ is the area crossed by the bubbles. The superficial velocity of bubbles, as indicated by Baumgarten et al. (5), is a function of bubble size and is different at each layer of the fluidized bed. They observed that the size of a bubble grows as it moves away from the distributor. To avoid this complexity one can assume that there is a mean bubble velocity $\bar{V}_b$ which is constant throughout the section below L_{mf}. One may then write

$$G = G_b + G_{mf} \tag{5}$$

Substituting $G = VS$ into Equation (5) and rearranging one obtains

$$S' = \frac{S(V_b - V)}{\bar{V}_b - V_{mf}} \tag{6}$$

The volume occupied by bubbles below L_{mf} is

$$\text{Vol}_b = L_{mf}\,(S - S') \tag{7}$$

Substituting Equation (6) into Equation (7) one gets

$$\text{Vol}_b = \frac{S\,L_{mf}\,(V - V_{mf})}{V_b - V_{mf}} \tag{8}$$

The mass of particles in the falling-density zone becomes

$$M_{s_1} = \rho_s\,\text{Vol}_{s_1} = \rho_s(1 - \epsilon_{mf})\frac{S\,L_{mf}\,(V - V_{mf})}{\bar{V}_b - V_{mf}} \tag{9}$$

and the mass in the lower zone

$$M_{s_2} = M - \frac{\rho_s(1 - \epsilon_{mf})S\,L_{mf}(V - V_{mf})}{\bar{V}_b - V_{mf}} \tag{10}$$

When one substitutes Equation (10) into Equation (2) the average density for the lower-density zone becomes

$$\bar{\rho}_d = \rho_{mf} - C\,(V - V_{mf}) \tag{11}$$

where

$$C = \frac{\rho_{mf}}{(\bar{V}_b - V_{mf})}$$

and

$$\frac{\rho_{mf}}{\rho_s} = 1 - \epsilon_{mf}$$

Since the average bubble velocity through the bed below L_{mf} has been assumed constant, C in Equation (11) is a constant and the average density in the constant-density zone has a linear relationship with the superficial air velocity. The data plotted on Figure 4 confirm this linear relationship between $\bar{\rho}_d$ and $(V - V_{mf})$ fairly well with the static bed height showing only a slight effect.

Using the least squares method one can obtain the intercepts and slopes of the straight lines from the experimental data. The equations which relate $\bar{\rho}_d$ with $(V - V_{mf})$ for 3M glass beads used are as follows:

(i) For 40- to 45-mesh glass beads:

$$\bar{\rho}_d = 1.371 - 0.00536\,(V - V_{mf,\ 40\ \text{mesh}}) \tag{12}$$

(ii) For 80- to 100-mesh glass beads:

$$\bar{\rho}_d = 1.269 - 0.00439\,(V - V_{mf,\ 80\ \text{mesh}}) \tag{13}$$

(iii) For 60- to 70-mesh glass beads:

$$\bar{\rho}_d = 1.300 - 0.00577\,(V - V_{mf,\ 60\ \text{mesh}}) \tag{14}$$

where $\bar{\rho}_d$ is in gram per cubic centimeter.

Bed-Density Correlation in the Falling-Density Zone

The fluidized bulk density in the falling-density zone decreased as the height from the distributor increased. For the experimental runs at low air velocity the density distribution in this falling zone was approximately represented by the one-tailed normal distribution function, when one considers that the falling-density zone started at the location corresponding to the static bed height:

$$\frac{\rho}{\rho_{pa}} = \frac{1}{\sqrt{2\pi}\sigma}\exp\left[-\frac{\left(\frac{h}{L_{mf}} - 1\right)^2}{2\sigma^2}\right] \tag{15}$$

The variance σ^2 from all the runs at low air velocity were correlated as a function of the major variables of the operation and the beds as follows (Figure 5):

$$\sigma^2 = 2.117 \times 10^{-7}\left(\frac{V\,\rho_F\,D_p}{\mu}\right)^{1.278}\left(\frac{D_p}{D_c}\right)^{-1.985}\left(\frac{L_{mf}}{D_c}\right)^{-0.8933} \tag{16}$$

For the falling density zone distribution obtained from the bed fluidizing at higher air velocity the axial-density profile became rather skewed. Therefore the two-parameter (or two-indices) correlation with the following form was also used:

$$\rho/\rho_{pa} = A_o \exp B\,(h/L_{mf} - 1)^2 \tag{17}$$

At a height corresponding to L_{mf} (the position at prefluidized state) the fluidized bulk density is ρ_d, which is obtained from the axial-density profile (Figure 3). Except for shallow beds it was approximately the same as $\overline{\rho_d}$, the average density in the constant-density zone. The value of A_o in Equation (17) is then equal to ρ_d/ρ_{pa}, which was calculated for each condition.

Taking logarithms of both sides of Equation (17), one gets the following linear equation:

$$\text{Log}\ (\rho/\rho_{pa}) = \log\ (\rho_d/\rho_{pa}) + B\ (h/L_{mf} - 1)^2 = A + B\ (h/L_{mf} - 1)^2 \quad (18)$$

The relations developed above, Equations (15) and (18), hold better for low than high gas velocities in all cases. The two-parameter fit of Equation (18) however is a significant improvement over the one-tailed normal distribution represented by Equation (15). Although the linear correlation of the dimensionless density to the dimensionless height was not as good for the runs fluidizing at higher air velocities as that at lower velocities, it was possible to obtain a best straight line by using the method of least squares. Thus the slope B and the intercept $A = \log\ (\rho_d/\rho_{pa})$ can be found for all sets of experimental data fluidizing at various conditions.

The index B converges to a single value as the air velocity increases. This indicates that, at high air velocity, the particles carried up by the air bubbles are uniformly dispersed in the falling-density zone. No matter what the original static bed height, the value of index B is the same if it is fluidized at high air velocity. The effect of the static bed height on aggregative fluidization is pronounced only at low air velocity close to the minimum velocity of fluidization. The plot of index B vs. the particle size shows that the particle size affects the state of aggregative fluidization only at lower air velocities. In other words the particles are distributed in a similar manner over the falling-density zone (at high air velocity), no matter what size of particles make up the bed.

The value of A, which is actually the logarithm of the ratio of fluidized bulk density at the position of the static bed height to the bulk density of the same particles in their packed state, was correlated in a similar way as for index B. In all cases the effect of static bed height on the index A was significant when $L_{mf}/D_c < 1$. When this ratio was greater than one, the fluidized bed expansion was almost the same for all static bed heights fluidizing at the same air velocity. For the 80- to 100-mesh glass beads the index A correlation with air velocity converges to one curve for all static bed height, even when L_{mf}/D_c is less than one. This indicates that when the particles size is small, the entrance effect has little effect on index A.

Index B and index A (which is used to describe the state of aggregative fluidization) can be correlated as functions of the operating variable and the characteristics of the bed and particles. The following dimensionless equations were derived from data obtained:

$$|A| = 1.396 \times 10^{-5}\left(\frac{D_p V \rho_F}{\mu}\right)^{0.978} (D_p/D_c)^{-1.265}\ (L_{mf}/D_c)^{0.3469} \quad (19)$$

$$|B| = 5.492 \times 10^{9}\left(\frac{D_p V \rho_F}{\mu}\right)^{-2.094} (D_p/D_c)^{3.045}\ (L_{mf}/D_c)^{0.3474} \quad (20)$$

Bakker and Heertjes (3) also proposed a two-parameter correlation of the falling-zone density but indicated that only one of the parameters is a function of the fluidizing gas velocity.

The effect of bed composition on the values of index A and index B is shown in Figure 6. The beds were originally at a static height of 6.5 in and were composed of various fractions of 40- to 45-mesh and 80- to 100-mesh particles. They were fluidized at an air velocity of 60 ft./min. The axial density profiles were obtained and index A and index B calculated for every bed composition. Bed compositions of 0, 2, 5, 10, 50, 90, 95, 98, and 100% by weight of 40- to 45-mesh glass beads were used. The results show that the mixing of particles of different sizes affects index A and index B significantly only when the composition is below 10% or above 90% by weight of 40- to 45-mesh glass beads. Figure 6 indicates that at these compositions the axial density profiles have the forms closest to the ideal fluidized beds. This result is consistent with the observation of Bailie et al. (1, 2), Dotson (7), and Baumgarten and Pigford (5) on the stability of fluidized beds.

Effect of Distributor

Only one type of gas distributor (canvas filter cloth) was used in this investigation. Groshe (10) studied the effect of the distributor using a similar experimental technique. He did not carry out his investigations of density profiles to include the falling zone. His results show that for the lower region the density remained relatively constant for a good distributor but behaved erratically for a poor distributor and did not remain constant. This indicates that the two-zone model does not represent the physical situation when poor distribution of the gas is obtained.

Determination of the Fluidized Bed Height

The behavior of gas-solid fluidized beds observed in this work deviated considerably from the behavior of an ideal expansion of a packed bed. The particles were not as uniformly suspended in the bed as is usually observed in most of the liquid fluidized beds. The two-phase model for gas-solid fluidization is only a very approximate one. Actually there was no

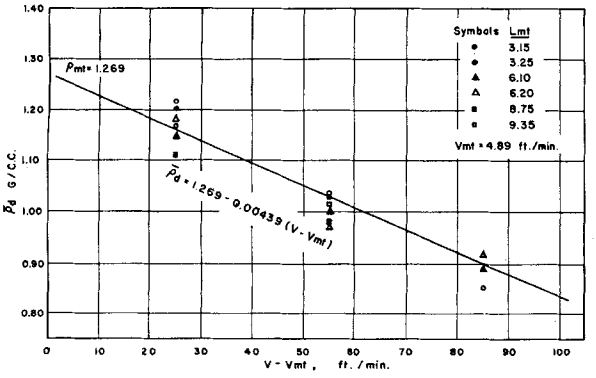

Fig. 4. ρ_d correlation for 80- to 100-mesh glass beads.

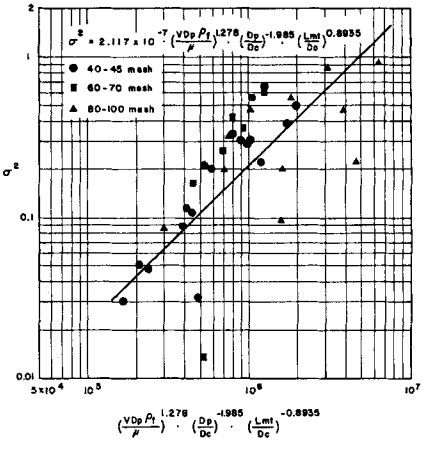

Fig. 5. Dimensionless correlation for variance falling-zone density.

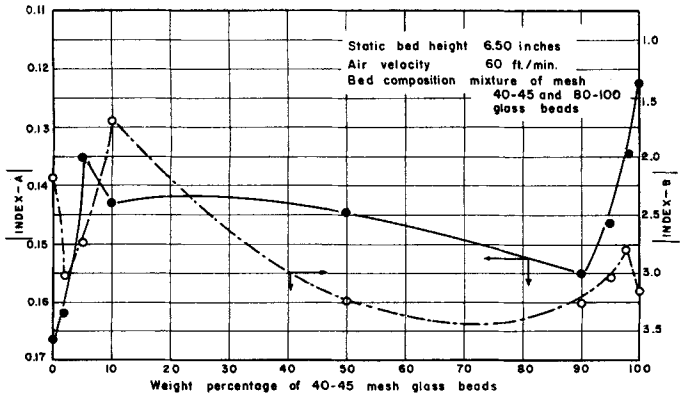

Fig. 6. Effect of bed composition on indices *A* and *B*.

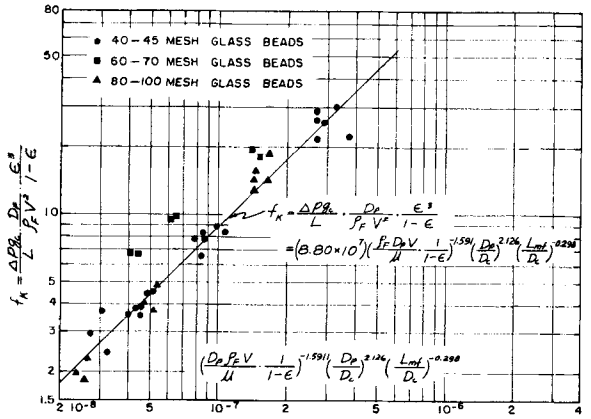

Fig. 8. Dimensionless correlation of friction factor with bed height determined by method 2.

distinct phase which could be defined as a bubble phase consisting of purely gases, nor was there a dense phase consisting of uniform emulsion of particles. The bubbles, formed by gas and held in the pore spaces between solids, grow in size as they rise from gas distributor toward the top of the bed, and finally burst near the position corresponding to the static bed height. The small-size particles suspended in the air stream were fluctuating and weaving at the top of the bed, and the disperse phenomenon dominated the top of the bed. Therefore the fluidized bed height could not be measured visually. This was also pointed out by Groshe (*10*) in his work.

Three methods can be used to define the fluidized bed height.

1. End point of density profile: Point the density of the bed goes to zero. This corresponds to the maximum height observed visually.

2. Cross point of the density profile: Point the ideally expanded bed profile crossed the actual density profile. This is shown as a dotted line on Figure 3. The particles are assumed to be uniformly distributed below this height, and the significance of the portion above this to the over-all performance of the bed is considered negligible. This height, as defined, should signify the bed, though aggregative, as a particulate one.

3. Height determined by IIS method: The index of stability (IIS), as proposed by Bailie et al. (*1, 2*), is a measure of the magnitude of the fluidized bed density fluctuations. The breaking point or point of maximum instability may be used to define the fluidized bed height. This corresponds closely to the height determined by method 2.

In the calculation for reactor conversion the bed height defined in (2) and (3) should give a more realistic picture, since the insignificant part of the disperse phase is neglected in this consideration.

The fractional fluidized bed expansion is plotted as a function of superficial air velocity with L_{mf}/D_c as the parameter for bed heights as defined by method 1 in Figure 7. Figure 7 shows a linear relationship consistent with data presented by Minit et al. (*16*). Method 2 deviated considerably from a linear relationship.

Pressure Gradient Correlations

A typical pressure drop flow diagram obtained in this work resembled in shape the pressure drop flow diagram for ideally fluidizing systems (*13*); that is the pressure drop became essentially just the weight of the bed per unit cross section just beyond the minimum velocity of fluidization. This indicates that the tube-bundle theory (*6*) developed for the study of the pressure drop through a packed bed may be applied analogously to the analysis of the pressure gradient in the present fluidizing systems, provided the fluidized bed height can be correctly determined. Since the pressure drop ΔP remained constant but the bed height increased at air flows beyond the minimum fluidizing velocity, the pressure gradient $\Delta P/L$ decreased with the increase in air velocity.

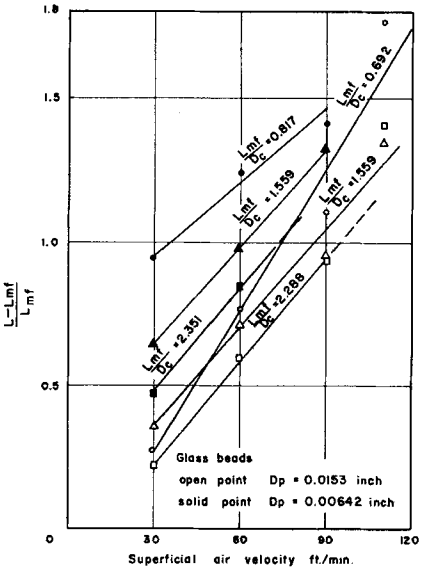

Fig. 7. The fractional fluidized bed expansion from height determined by method 1.

In Figure 8 the pressure gradients $\Delta P/L$ are correlated in a form of friction factor f_k originally proposed (*8*) for correlating the pressure drops through packed beds against the modified Reynolds number $N_{Re}' = \frac{D_p V \rho_F}{\mu} \cdot \frac{1}{1-\epsilon}$. The numerical values of the pressure gradient $\Delta P/L$ for fluidized beds depend on the definition of fluidizing bed height used. The correlation obtained with height determined by method 1 yields curves that resemble the Ergun equation for packed beds (*6*) and with bed height determined by method 2, the Blake-Kozeney equation. In both cases the effect of particle D_p appears to be more pronounced than indicated by the correlations proposed for packed beds.

The results of the dimensionless analysis and modifications as suggested by the previous workers (*11*) lead to the form

$$f_K = \frac{g_c \Delta P}{L} \cdot \frac{\epsilon^3}{1-\epsilon} \cdot \frac{D_p}{\rho_F V^2} = C\left(\frac{D_p \rho_F V}{\mu} \cdot \frac{1}{1-\epsilon}\right)^a \left(\frac{D_p}{D_c}\right)^b \left(\frac{L_{mf}}{D_c}\right)^c \quad (21)$$

where the constants, a, b, and c can be evaluated from the experimental data with the height of fluidized bed defined by methods 1 and 2.

With the height defined by method 1:

$$f_K = \frac{g_c \Delta P}{L} \cdot \frac{\epsilon^3}{1-\epsilon} \cdot \frac{D_p}{\rho_F V^2} = (9.028 \times 10^5)\left(\frac{D_p \rho_F V}{\mu} \cdot \frac{1}{1-\epsilon}\right)^{-0.945} \left(\frac{D_p}{D_c}\right)^{1.389} \left(\frac{L_{mf}}{D_c}\right)^{-0.224} \quad (22)$$

With the height defined by method 2:

$$f_K = \frac{g_c \Delta P}{L} \cdot \frac{\epsilon^3}{1-\epsilon} \cdot \frac{D_P}{\rho_F V^2} = (8.80 \times 10^7) \left(\frac{D_P \rho_F V}{\mu} \cdot \frac{1}{1-\epsilon}\right)^{-1.591} \left(\frac{D_P}{D_c}\right)^{2.126} \left(\frac{L_{mf}}{D_c}\right)^{-0.298} \quad (23)$$

Equation (23) is plotted in Figure 8. The height determined by method 1 gives more scattered correlation than that determined by method 2. It may be concluded, in the proposed dimensionless correlation of pressure gradient through fluidized bed, that the height determined by method 2 gives more consistent result than that determined by method 1.

DISCUSSION AND CONCLUSIONS

Many studies of heat and mass transfer in packed beds have appeared in the literature. Investigators in the field of fluidization have attempted packed bed types of correlations in the study of fluidized bed reactors but encountered difficulties due to the nonuniform particle distribution throughout the bed. The reacting gas flowing through the fluidized bed is not only a tortuous flow through the constant void space as in packed beds, but in addition it is affected by the impacts between particles and the interaction between particles and the flowing medium. A quantitive measurement of the complexity of the flowing pattern in the fluidized bed is therefore important. The mass and heat transfer in the fluidized bed is governed by the surface area and the movement of particles in the bed. Data have shown that the transfer is better in the locations where the solid particles are dense and are constantly circulating.

Mickley et al. (*14*) in their study of heat transfer for gas fluidized beds conclude: "The local time-mean wall-to-bed heat transfer coefficient varies with the axial position of heat transfer surface, decreasing above the bottom of the bed. On the other hand, the local coefficient is not significantly influenced by total height of the bed." This observation is at least in qualitative agreement with the observation made in this work for the axial particles distribution profiles.

Shirai et al. (*17*) drew the same conclusion in studying the axial distribution of heat transfer coefficients. The axial distribution of particles-to-fluid heat transfer coefficients obtained by them is almost identical in shape to the axial-density profile obtained in this work.

The two-zone concept of fluidization appears to represent the physical picture of the axial-density profile for a fluidized bed under most operating variables studied. The model holds particularly well for beds with a good gas distributor and low velocities. For high gas velocities and poor distributors, that is very poor fluidization, the model begins to break down. The close relationship between the axial distribution of the heat transfer coefficient and the axial-density profile suggests that the study of the two-zone density profile of fluidized beds will help in understanding heat and mass transfer mechanism in the fluidized bed.

NOTATION

A_o = constant, dimensionless
A_r = projected area of γ-beam path, L^2
b = build-up factor
A = index of fluidized bed, dimensionless
B = index of fluidized bed, dimensionless
C = constant
D_c = inner diameter of fluidized column, L
D_p = diameter of particle, L
f_K = friction factor, dimensionless
G = volumetric air velocity, L^3/θ
G_b = volumetric bubble velocity, L^3/θ
g_c = conversion from force to mass, $mL/F\theta^2$
G_{mf} = volumetric velocity of minimum fluidization, L^3/θ
h = height above the distribution in bed, L
I/I_o = fraction of photons remaining in the beam after passage through absorber of thickness d, dimensionless
L = height of fluidized bed L
L_{mf} = static (onset) height of bed, L
M = total particle weight in bed, m
M_{s_1} = weight of particles fluidizing above L_{mf}, m
M_{s_2} = weight of particles fluidizing below L_{mf}, m
N_{Re} = Reynolds number, $V \rho_F D_P/\mu$, dimensionless
N_{Re}' = modified Reynolds number, $V \rho_F D_P/\mu$. $L/1 - \epsilon$, dimensionless
ΔP = pressure drop through fluidized bed, F/L^2
S = cross-sectional area of the fluidized bed, L^2
S' = part of cross-sectional area of the fluidized bed, L^2
V = superficial air velocity, L/θ
$\overline{V}_b$ = average linear velocity of bubbles, L/θ
V_{mf} = minimum velocity of fluidization, L/θ
Vol_b = the volume occupied by bubbles below L_{mf}, L^3
Vol_{s_1} = volume of particles fluidizing above L_{mf}, L^3

Greek Letters

ϵ = porosity of the fluidized bed
ϵ_{mf} = porosity of the fluidized bed at onset fluidization, dimensionless
ρ = fluidized bulk density, m/L^3
ρ_d = fluidized bulk density at the position corresponding to the static bed height, m/L^3
$\overline{\rho_d}$ = average line density in the constant density zone, M/L^3
ρ_F = density of fluid, M/L^3
ρ_{mf} = fluidized bulk density at onset fluidization, M/L^3
ρ_{pa} = bulk density of bed at packed state, M/L^3
ρ_s = density of solid particle, M/L^3
σ^2 = variance
μ = viscosity of fluid, $m/L\theta$
μ_m = absorption coefficient, L^{-1}

LITERATURE CITED

1. Bailie, R. C., L. T. Fan, and J. J. Stewart, *Ind. Eng. Chem.*, **53**, 567 (1961).
2. ———, *J. Chem. Eng. Data*, **6**, 469 (1961).
3. Bakker, P. J., and P. M. Heertjes, *Brit. Chem. Eng.*, **3**, 240 (1958.
4. ———, *Chem. Eng. Sci.*, **4**, 12, No. 1 pp. 260-71 (1960).
5. Baumgarten, P. K., and R. L. Pigford, *A.I.Ch.E. Journal*, **6**, 115 (1960).
6. Bird, R. B., W. E. Stewart, and E. N. Lightfoot, "Notes on Transport Theory," Wiley, New York (1959).
7. Dotson, J. M., *A.I.Ch.E. Journal*, **5**, 169 (1959).
8. Ergun, S., and A. A. Orning, *Ind. Eng. Chem.*, **41**, 1179-84 (1949).
9. Furukawa, J., and T. J. Ohmae, *Ind. Chem. (Japan)*, **54**, 798-800 (1951).
10. Grohse, E. W., *A.I.Ch.E. Journal*, **1**, 358 (1955).
11. Leva, Max, "Fluidization," McGraw-Hill, New York (1959).
12. Massimilla, Leopoldo, and J. M. Westwater, *A.I.Ch.E. Journal*, **6**, 134 (1960).
13. Matheson, G. L., W. A. Herbst, and P. H. Hole, *Ind. Eng. Chem.*, **41**, 1099 (1949).
14. Mickley, H. S., D. F. Fairbank, and R. D. Hawthorn, *Chem. Eng. Progr. Symposium Ser. No. 32*, **57**, p. 51 (1961).
15. Minet, R. G., John Happel, and William Kapfer, *A.I.Ch.E. Journal*, to be published.
16. Morse, R. D., and C. O. Ballou, *Chem. Eng. Progr.*, **47**, 199 (1951).
17. Shirai, T., et al., "Heat Transfer in Gas Fluidized Beds," Tokyo Inst. Technol., Japan (1960).
18. Shuster, W. W., and Peter Kisliak, *Chem. Eng. Progr.*, **48**, 455 (1952).
19. Yasui, George, and L. N. Johanson, *A.I.Ch.E. Journal*, **4**, 445 (1958).

Manuscript received July 11, 1961; revision received October 17, 1961; paper accepted October 23, 1961.